Edge diffraction, trace formulae and the cardioid billiard

Henrik Bruus† and Niall D Whelan‡§

† Centre de Recherches sur les Très Basses Températures, CNRS, BP 166, F-38042 Grenoble Cédex 9, France
‡ Centre for Chaos and Turbulence Studies, Niels Bohr Institute, Blegdamsvej 17, DK-2100, Copenhagen Ø, Denmark

Abstract. We study the effect of edge diffraction on the semiclassical analysis of two-dimensional quantum systems by deriving a trace formula which incorporates paths hitting any number of vertices embedded in an arbitrary potential. This formula is used to study the cardioid billiard, which has a single vertex. The formula works well for most of the short orbits we analysed but fails for a few diffractive orbits due to a breakdown in the formalism for certain geometries. We extend the symbolic dynamics to account for diffractive orbits and use it to show that in the presence of parity symmetry the trace formula decomposes in an elegant manner such that for the cardioid billiard the diffractive orbits have no effect on the odd spectrum. Including diffractive orbits helps resolve peaks in the density of even states but does not appear to affect their positions. An analysis of the level statistics shows no significant difference between spectra with and without diffraction.

PACS numbers: 0320, 0365S, 0545

1. Introduction

Periodic orbit theory [1] provides a method of relating local, canonically invariant information about classical periodic orbits to global quantum information such as the density of states. However, this theory must be extended if the classical mechanics is not defined due to discontinuities. There is one class of discontinuity which is relatively mild in that all trajectories are well defined but just their behaviour changes abruptly at some points in phase space. Examples of this include grazing angles in billiards [2, 3] and the circle–straight joint in the Bunimovich stadium [4, 5]. A more severe discontinuity is one in which some trajectories are undefined. Examples of this include the vertex of a wedge [6, 7, 8, 9] and three body collisions [10] since in neither case can we continue a trajectory through the discontinuity. Other examples of discontinuities include scattering singularities [11], flux tubes [12, 13] and small scattering disks [13, 14]. In each case, periodic orbit theory can be extended by incorporation of so-called diffractive effects—in the case of vertices this is called edge diffraction. To incorporate the effect of a discontinuity, one compares to the solution of the local scattering problem. For the wedge this was solved by Sommerfeld [15] and the solution discussed in [16, 17].

The structure of the paper is as follows. In section 2 we derive a trace formula for diffractive orbits analogous to the Gutzwiller trace formula for ordinary orbits. The

§ New address: Division de Physique Théorique, IPN, 91406 Orsay Cédex, France.

amplitude of each diffractive orbit is affected by the curvatures it experiences on the geometric part of its path as well as by the diffraction at the vertex. As an example, we employ the theory in a numerical study of the cardioid billiard [18] which is ergodic [19], and in section 3 we discuss various properties of this billiard. The comparison of the theory and numerics takes place in section 4. A brief analysis of the spectral statistics of the cardiod billiard is presented in section 5, while section 6 contains the conclusion.

2. Trace formula for diffractive orbits

The semiclassical formula for the trace $g(E)$ of the Green function $G(E)$ of a chaotic Hamiltonian is [1]

$$g(E) \equiv \mathrm{Tr}G(E) = \frac{1}{i\hbar} \sum_{\gamma} \frac{T_{\gamma}}{\sqrt{\Lambda_{\gamma}} \mp 1/\sqrt{\Lambda_{\gamma}}} \exp\{i(S_{\gamma}/\hbar - \sigma_{\gamma}\pi/2)\} \qquad (1)$$

where the sum is over all periodic orbits, γ. The factors T_{γ}, S_{γ}, Λ_{γ} and σ_{γ} are the canonically invariant periods, actions, stabilities and Maslov indices of the orbit, γ respectively. (The canonical invariance of σ_{γ} is proved in [20].) The $-/+$ factor refers to whether the orbit is direct hyperbolic or inverse hyperbolic. We extract the density of states $\rho(E)$ from the trace through the identity $\rho(E) = -\mathrm{Im}[g(E)]/\pi$. Periodic orbits are singled out because they have a stationary phase with respect to small deviations. The requirement of stationary phase can also select other phase space structures [21] and we will henceforth refer to the orbits which enter (1) as 'geometric orbits' to distinguish from other possibilities.

Another process which can lead to a stationary phase is a trajectory which hits a vertex. While not a classical trajectory, it is still a path in the sense of path integrals [22] with an amplitude that can be found by comparison with the scattering solution of a wedge; we call such a path 'diffractive'. The asymptotic (in $\hbar$) contribution to the Green function of the Schrödinger equation arising from the path from x' to x via the vertex at ξ is [6, 16, 17]

$$G_d(x, x', E) \approx \frac{\hbar^2}{2m} d(\theta, \theta') G_f(x, \xi, E) G_f(\xi, x', E) \qquad (2)$$

where G_f is the Green function in the absence of the wedge and $d(\theta, \theta')$ is a diffraction constant. It equals

$$d(\theta, \theta') = -2\frac{\sin(\pi/\nu)}{\nu} \left\{ \frac{1}{\cos(\pi/\nu) - \cos((\theta - \theta')/\nu)} \pm \frac{1}{\cos(\pi/\nu) + \cos((\theta + \theta')/\nu)} \right\} \qquad (3)$$

where θ and θ' are measured with respect to the wedge normal (unlike in [8, 9]) and $\nu = \alpha/\pi$, α being the opening angle of the wedge as shown in figure 1(*a*). The $+/-$ sign refers to Neumann/Dirichlet boundary conditions. We will mainly be interested in $\alpha = 2\pi$ for which

$$d(\theta, \theta') = \sec\left(\frac{\theta - \theta'}{2}\right) \mp \sec\left(\frac{\theta + \theta'}{2}\right). \qquad (4)$$

Note that $d(-\theta, \theta') = \mp d(\theta, \theta')$ and that $d(0, 0) = 2$ for Dirichlet boundary conditions and 0 for Neumann. The factor $\hbar^2/2m$ appears in (2) because we are using energy dependent Green functions; it is absent if we use the Green functions of the Helmholtz equation in two dimensions. The Green functions of (2) all have units 1/[Energy][Length]^2.

For free motion in two dimensions, $G_f(x_2, x_1, E) = -i\hbar^2 H_0^{(+)}(k|x_2 - x_1|)/8m$, where $H_0^{(+)}$ is the outgoing Hankel function and $k = \sqrt{2mE}/\hbar$. This form of G_f is assumed in the derivation of the diffraction constant. However (2) is more general. In the presence of
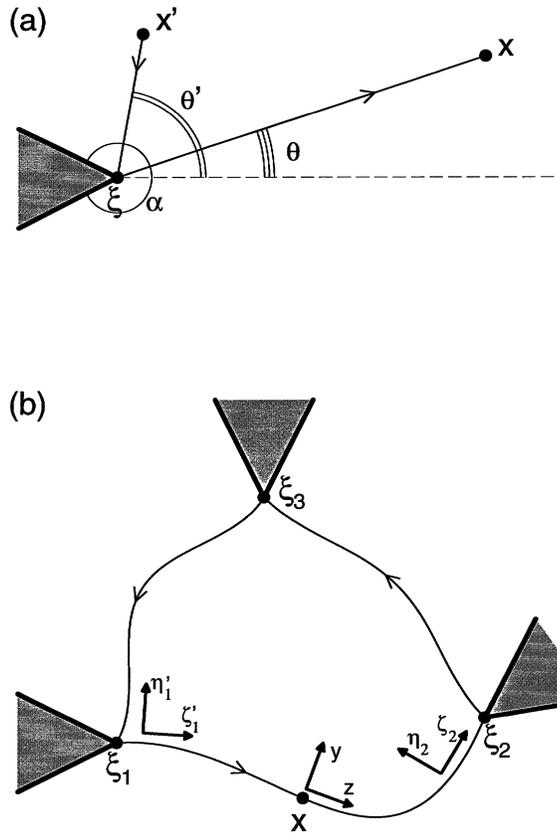
Figure 1. (*a*) A path connecting the point x' to the point x via the vertex ξ. The angles α, θ', and θ appear in (3) defining the diffraction constant. (*b*) A schematic diagram of a periodic diffractive orbit with its local coordinates.

a potential with a vertex, we tackle the local scattering problem by assuming the potential does not change much in a typical wavelength. We would then call the directions of the trajectory when it enters and leaves the vertex θ' and θ and use these in determining the diffraction constant $d(\theta, \theta')$. Away from the vertex, we connect the outgoing free space Green functions to the relevant semiclassical ones for that potential. For example, (2) is valid for the problem of motion bounded within a wedge in the presence of gravity [23] for which G_f is more complicated. For that reason, we do not assume billiard conditions in the subsequent discussion, although we do restrict the discussion to two spatial dimensions. The content of (2) and (3) is that an orbit entering the vertex can be continued out at any angle with a quantum amplitude given by $d(\theta, \theta')$. The contribution of such a diffractive orbit is of order $\sqrt{\hbar}$ relative to that of a geometric orbit. We now analyse this semiclassically to derive a trace formula in analogy to (1).

If there are n diffractions as sketched in figure 1(*b*), (2) generalizes to

$$G_d(x, x', E) \approx \left\{ \prod_i^n \frac{\hbar^2}{2m} d_i \right\} G_f(x, \xi_n) G_f(\xi_n, \xi_{n-1}) \cdots G_f(\xi_2, \xi_1) G_f(\xi_1, x') \tag{5}$$

where we have suppressed the energy dependence in G_f and the θ dependence in the diffraction constants. To obtain the trace, we first identify the points x and x' and then invoke stationary phase to require that the momenta also match smoothly—as for geometric orbits. Orbits which satisfy these constraints we call diffractive periodic orbits. They can be found, in principle, by firing out trajectories at all angles from all the vertices and determining which ones return to a vertex. We impose no constraint on the momenta at the vertices and so allow any incoming or outgoing angles.

To proceed, we define local coordinates along the various classical paths. At each point x, we take z and y to be the local coordinates parallel and transverse to the path, respectively. At each vertex we define local coordinates, ζ_i and η_i, on the the incoming path and ζ_i' and η_i' on the outgoing path. The local transverse momentum at x is p and the local transverse momenta at the vertex ξ_i are π_i and π_i'. The constant energy approximation to the classical Green function from any x_1 to any x_2 is [1]

$$G_f(x_2, x_1, E) \approx \frac{1}{i\hbar} \frac{1}{\sqrt{2\pi i\hbar}} D(x_2, x_1) \exp\{i(S/\hbar - \mu\pi/2)\}. \qquad (6)$$

The action S is evaluated along the path and μ counts the caustics along the orbit. The factor D equals [1]

$$D(x_2, x_1) = \frac{1}{|\dot{z}_2 \dot{z}_1|^{1/2}} \left| -\frac{\partial^2 S}{\partial y_2 \partial y_1} \right|^{1/2} = \frac{1}{|\dot{z}_2 \dot{z}_1|^{1/2}} \left| \left(\frac{\partial y_2}{\partial p_1} \right)_{y_1} \right|^{-1/2} \qquad (7)$$

where the subscript on the bracket of the second equation indicates that we take the derivative of the final position with respect to the initial momentum while holding the initial position fixed. This then defines a fan of initial conditions radiating from the source point x_1. This is the contribution of a single classical trajectory—if there is more than one, we must sum over them.

Evaluation of the trace involves integrating along the periodic orbit and transverse to it. The integral along the orbit can be done one arc at a time and below we consider just the arc between ξ_1 and ξ_2. Equations (6) and (7) imply

$$G_f(\xi_2, x)G_f(x, \xi_1) \approx \left(\frac{1}{i\hbar} \frac{1}{\sqrt{2\pi i\hbar}} \right)^2 D(\xi_2, x)D(x, \xi_1) \exp\left\{ i \left[S_{21}/\hbar - (\mu_2 + \mu_2)\pi/2 \right] \right\} \quad (8)$$

where $S_{21} = S_2 + S_1$ is the action of the path between ξ_1 and ξ_2 via x. At each point, x, along the orbit, we calculate the transverse y integral. The only y dependence, to leading order in $\hbar$, is in the action which we approximate as

$$S_{21} \approx S_{21}^0 + \frac{1}{2} \frac{\partial^2 S_{21}}{\partial y^2} y^2. \qquad (9)$$

The partial derivative is taken while holding the initial and final coordinates η_1' and η_2 fixed at zero. S_{21}^0 is the action evaluated at $y = 0$ and is independent of the position z along the orbit. The stationary phase integral yields

$$\int_{-\infty}^{\infty} dy \exp\left(iS_{21}/\hbar\right) = \sqrt{2\pi i\hbar} \left| \frac{\partial^2 S_{21}}{\partial y^2} \right|^{-1/2} \exp\left(i(S_{21}^0/\hbar - \sigma\pi/2)\right) \qquad (10)$$

where σ is zero if the second derivative in (9) is positive and is unity if the second derivative is negative.

We now seek to manipulate the various partial derivatives which come from the two amplitude factors D and from the stationary phase integral (10). These all come with a

power of $\frac{-1}{2}$ and with absolute value signs. For purposes of manipulation, we neglect those for the moment so the combination we need to analyse is

$$\left(\frac{\partial y}{\partial \pi_1'}\right)_{\eta_1'} \left(\frac{\partial y}{\partial \pi_2}\right)_{\eta_2} \frac{\partial^2 (S_1 + S_2)}{\partial y^2} = \left(\frac{\partial y}{\partial \pi_1'}\right)_{\eta_1'} \left(\frac{\partial y}{\partial \pi_2}\right)_{\eta_2} \left(\left(\frac{\partial p}{\partial y}\right)_{\eta_1'} - \left(\frac{\partial p}{\partial y}\right)_{\eta_2}\right). \tag{11}$$

We have used the fact that the derivative of the action with respect to the final position equals the final moment while the derivative with respect to the initial position equals the negative of the initial momentum. Also, we have inserted all of the relevant subscripts to indicate what is being kept fixed in each derivative. We now show that this factor is independent of position along the orbit. We can combine partial derivatives in (11) to obtain

$$\left(\frac{\partial y}{\partial \pi_2}\right)_{\eta_2} \left(\frac{\partial p}{\partial \pi_1'}\right)_{\eta_1'} - \left(\frac{\partial y}{\partial \pi_1'}\right)_{\eta_1'} \left(\frac{\partial p}{\partial \pi_2}\right)_{\eta_2} = \left(\frac{\partial (y, p)}{\partial (\pi_2, \pi_1')}\right)_{\eta_1', \eta_2}. \tag{12}$$

In the right half of (12) we have borrowed the Jacobian notation of [24]. (We have made use of the trivial freedom to specify that in the first derivative of the left hand side we are also holding η_1' fixed, with similar specifications in all four terms.) To determine the value of this Jacobian corresponding to some different point z' along the trajectory, we should multiply (12) by the Jacobian relating the transverse variables variables (y, p) at position z to the transverse variables (y', p') position z'. However, because these variables are transverse to a trajectory, their Jacobian is identically unity; the two sets of variables are canonically related owing to symplectic nature of the Hamiltonian flow. It follows that the combination of factors appearing in (11) is independent of position z'. In particular, it is particularly convenient to calculate it very close to one of the vertices. If z is such that the point is close to ξ_2, we have

$$\left(\frac{\partial y}{\partial \pi_2}\right)_{\eta_2} = 0 \qquad \left(\frac{\partial p}{\partial \pi_2}\right)_{\eta_2} = 1. \tag{13}$$

It follows that

$$\left(\frac{\partial (y, p)}{\partial (\pi_2, \pi_1')}\right)_{\eta_1', \eta_2} = -\left(\frac{\partial y}{\partial \pi_1'}\right)_{\eta_1'} \tag{14}$$

where the right hand side is evaluated at the point ξ_2. Henceforth, we change notation slightly and call this term $\partial \eta_2 / \partial \pi_1'$ to stress that it is evaluated at the second vertex. This factor is simply the spread in position at ξ_2 of a fan of trajectories radiating from ξ_1.

We also want that the phase index, $\mu_1 + \mu_2 + \sigma$ be independent of position along the orbit. It is not true that the indices are separately invariant; it is simple to imagine that as we change position z along the orbit, we will gain or lose caustics in going from the two vertices to the intermediate position. However, these changes will be exactly mirrored by changes in the index σ such that the sum is invariant. For a demonstration of this, we refer to [25] where the authors evaluate an integral similar to (5). They interpret (6) as a propagator along the orbit with z playing the role of time. Using the semigroup property of time-dependent propagators, they conclude that the phase index is a constant. Since this is constant, we are free to use μ_{21} which is the number of caustics of a fan of trajectories going from vertex 1 to vertex 2.

That completes the y integral. For the z integral, we remark that the only z dependence is in the velocity $|\dot{z}|^{-1/2}$ which appears in the amplitudes D of (8). Since there are two of them, the integral to be performed is simply

$$\int \frac{\mathrm{d}z}{|\dot{z}|} = T_{21} \tag{15}$$

which is just the time it takes to get from ξ_1 to ξ_2. Putting together all the remaining factors, we conclude that

$$
\int dz\,dy\,G_f(\xi_2, x)G_f(x, \xi_1) \approx \frac{T_{21}}{(i\hbar)^2\sqrt{2\pi i\hbar}} \frac{1}{|\dot{\zeta}_2\dot{\zeta}_1|^{1/2}} \left|\frac{\partial\eta_2}{\partial\pi_1'}\right|^{-1/2} \exp\{i(S_{21} - \mu_{21}\pi/2)\}
$$

$$
= \frac{T_{21}}{i\hbar} G_f(\xi_2, \xi_1), \tag{16}
$$

where we have used (6) and (7) in the second line and dropped the superscript 0 on the action.

The appealing fact that the trace integral on the arc between ξ_1 and ξ_2 is proportional to the Green function between these points simplifies the analysis tremendously. Recall that we must still multiply all of the other free Green functions from (5) so there is a factor which is simply the product of all the Green functions from vertex to vertex. In doing the integrals along the arc between ξ_i and ξ_{i+1}, we get exactly the same product but multiplied by $T_{i+1,i}$ so that the integral of (5) is

$$
g_\gamma(E) = \frac{T_\gamma}{i\hbar}\left\{\prod_{i=1}^{n_\gamma}\left(\frac{\hbar^2}{2m}\right)d_i G(\xi_{i+1}, \xi_i)\right\}
$$

$$
= \frac{T_\gamma}{i\hbar}\left(\frac{\hbar}{8\pi m^2}\right)^{n_\gamma/2}\left\{\prod_{i=1}^{n_\gamma}\frac{d_i}{|\dot{\zeta}_i|}\left|\frac{\partial\eta_{i+1}}{\partial\pi_i'}\right|^{-1/2}\right\}\exp\{i(S_\gamma/\hbar - \sigma_\gamma\pi/2 - 3n_\gamma\pi/4)\}, \tag{17}
$$

where S_γ, T_γ and σ_γ are the sums of $S_{i+1,i}$, $T_{i+1,i}$ and $\mu_{i+1,i}$ along the orbit. The velocity $\dot{\zeta}_i$ is given by energy conservation and is a constant at each vertex and the index i is cyclic so vertex $n + 1$ is identified with vertex 1. This diffractive trace formula is the main result of this section. The formula was given in [6] by comparison with creeping diffraction, where Watson contour integration [2] can be used to show that the trace has the same structure. The diffractive trace formula is similar to the Gutzwiller trace formula (1) but is suppressed by a relative factor of $\hbar^{n/2}$ [21]. (17) only shows the contribution of a single diffractive orbit; in practice we must sum over all such orbits and so introduce the subscript γ to distinguish them. If the orbit is a repeat of a shorter primitive orbit, the factor of T in (17) is the period of the primitive orbit.

We now specialize to the potential-free case so that $\hbar = m = 1$, $S/\hbar = kL$, $T = L/k$, $E = k^2/2$, and $|\dot{\zeta}_i| = k$. We further invoke the infinitesimal relation $\delta\pi_i' = k\delta\phi_i'$ where $\delta\phi_i'$ is the angular deviation from the periodic orbit on leaving vertex ξ_i so that

$$
\left|\frac{\partial\eta_{i+1}}{\partial\pi_i'}\right| = \frac{1}{k}\left|\frac{\partial\eta_{i+1}}{\partial\phi_i'}\right| \equiv \frac{1}{k}F_i. \tag{18}
$$

The contribution to the density of states in k is given by $\rho_\gamma(k) = -k\text{Im}[g_\gamma(E)]/\pi$ so

$$
\rho_\gamma(k) = \frac{L_\gamma}{\pi}\left\{\prod_i^n\frac{d_i}{\sqrt{8\pi k F_i}}\right\}\cos\left(kL_\gamma - \sigma_\gamma\pi/2 - 3n_\gamma\pi/4\right) \tag{19}
$$

to be contrasted with

$$
\rho_g(k) = \frac{L_g}{\pi}\frac{1}{\sqrt{\Lambda_g}\mp 1/\sqrt{\Lambda_g}}\cos\left(kL_g - \sigma_g\pi/2\right) \tag{20}
$$

for geometric orbits. In (19), the factor F_i has a simple interpretation; if we launch a narrow cone of trajectories from vertex ξ_i centered on the periodic orbit, F_i gives the width of the cone when it arrives at ξ_{i+1} [7]. This interpretation in terms of cones is in contrast with that of cylinders for geometric orbits. (19) was also obtained in [8] for the special

case of straight walls everywhere so that $F_i = L_i$, the distance between the vertices. We also mention that this analysis applies equally well if two of the diffraction points, ξ_i, are at the same vertex. In particular, if there is only one vertex, then the diffractive periodic orbits are those which leave the vertex and return to it following a classical path. (17) and (19) are true regardless of whether the classical motion is chaotic or not, although they are restricted to isolated diffractive orbits.

There is a zeta function [26] corresponding to (17) in analogy to that which exists for geometric orbits [27]. We start by defining the diffractive weight for each diffractive orbit

$$
t_\gamma = \left(\frac{\hbar}{8\pi m^2}\right)^{n_\gamma/2} \left\{\prod_i^{n_\gamma} \frac{d_i}{|\zeta_i|} \left|\frac{\partial \eta_{i+1}}{\partial \pi_i'}\right|^{-1/2}\right\}_\gamma \exp\left\{i(S_\gamma/\hbar - \sigma_\gamma \pi/2 - 3n_\gamma \pi/4)\right\} \tag{21}
$$

where we have now introduced the subscript γ to distinguish diffractive orbits. The sum over diffractive orbits is then

$$
g_d(E) = \sum_\gamma \frac{T_\gamma}{i\hbar} \sum_{r=1}^\infty t_\gamma^r = \sum_\gamma \frac{T_\gamma}{i\hbar} \frac{t_\gamma}{1 - t_\gamma} \tag{22}
$$

where we have organized the sum into the primitive orbits and their repeats. To leading order in $\hbar$,

$$
\frac{dt_\gamma}{dE} \approx -\frac{T_\gamma}{i\hbar} t_\gamma \tag{23}
$$

so that

$$
g_d(E) = \frac{d}{dE} \log\left(\prod_\gamma (1 - t_\gamma)\right). \tag{24}
$$

The quantity $\zeta_d^{-1}(E) = \prod_\gamma (1 - t_\gamma)$ is the diffractive zeta function to the power -1. When multiplied by the corresponding geometric zeta function [2] to the power -1 and appropriately regulated [28, 29], the product equals the spectral determinant $\prod_n (E - E_n)$ so that its zeros give the quantum energy levels. Due to the regularization, the zeros of the separate terms in $\zeta_d^{-1}(E)$ are not true zeros of the product. A formula analogous to (24) also holds in the case of billiards [6, 9].

The function $\zeta_d^{-1}(E)$ involves only a single product over periodic orbits. In contrast, the zeta function for geometric orbits has an additional product over an integer index which can be thought of as labeling local eigenstates transverse to each orbit [30]. Near the orbit, these local eigenstates typically have the form $\psi_n(y) \sim y^n$ with $n \geq 0$. We conclude that diffractive orbits have only the $n = 0$ local eigenstate. Higher states do not exist because they would have a node on the periodic orbit and would not be affected by the diffraction. This was also noted in the scattering geometries discussed in [7, 9] where it caused there to be no lower families of quantum resonances. This difference is intimately related to the fact that the Green functions in (5) are multiplicative [2] in contrast to the behaviour of Green functions for geometric orbits [1].

3. The cardioid billiard

In this section, we discuss various aspects of the cardioid billiard which are relevant to us. We briefly review its classical properties and construct the symbolic dynamics for the geometric orbits and diffractive orbits. The Maslov indices are given by a simple rule in terms of the symbolical dynamics. We then discuss the role of symmetry in the quantum problem and how the geometric and diffractive trace formulas conspire to give the even and odd spectra. We conclude with a discussion of the Weyl formula.
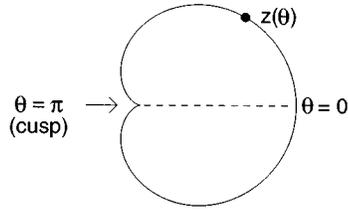
Figure 2. The cardioid billiard. A generic point $z(\theta)$ at the perimeter is shown as well as the two special points $\theta = 0$ and $\theta = \pi$ (the cusp). We restrict θ to the interval $[-\pi, \pi)$. The dashed line indicates the symmetry axis.

3.1. Classical mechanics

We study the cardioid billiard whose boundary is defined by the following mapping of the unit circle in the complex plane

$$z(\theta) = e^{i\theta} + \frac{1}{2} e^{i2\theta} \qquad \theta \in [-\pi, \pi) \tag{25}$$

and is plotted in figure 2. The angle θ is defined such that it changes discontinuously from π to $-\pi$ at the cusp. If the factor of $1/2$ is replaced by a parameter, b this represents a family of billiards introduced in [18] and subsequently studied exhaustively [19, 31, 32, 33, 34, 35]. For $b < 1/2$, (25) is a conformal mapping but is not strictly conformal for $b = 1/2$ since the derivative of z with respect to θ vanishes at $\theta = \pi$. In practice, this does not matter and the algorithm introduced in [33] to find the quantum eigenvalues still applies and was used by us. For $b > 1/2$ the curve crosses itself near $\theta = \pi$ and the billiard is not well defined. We note that the quantum behaviour of the cardioid was recently studied in [36]. The dynamics in the billiard consists of free motion within the domain followed by equal angle (specular) reflections at the boundary. Trajectories which strike the vertex are not defined but these are of measure zero. Motion in the cardioid has been proven by Markarian to be ergodic [19]. It is similar to the Bunimovich stadium [37] in that it is defocusing. Defocusing means that each point on the billiard has positive curvature so that parallel rays striking the boundary are initially focused. However, the billiard geometry is such that the trajectories typically diverge even more after the focal point resulting in a net defocusing. It is this mechanism which leads to the average divergence of trajectories and to chaos. In contrast, a dispersing system such as the Sinai billiard [38] has negative curvature so that initially parallel rays striking the boundary are immediately dispersed.

The curvature of the cardioid is

$$\kappa(\theta) = \frac{3}{4} \sec\left(\frac{\theta}{2}\right) \tag{26}$$

which is positive for all θ, as in a circle. For b somewhat less than $1/2$, the region near $\theta = \pi$ is dispersing rather than defocusing. Billiards with mixed focusing properties like this are difficult to analyse mathematically [19, 39] and it is for this reason that Markarian's proof works only for the cardioid. In cartesian coordinates near the cusp the billiard boundary satisfies the equation

$$y \approx \pm \frac{1}{2} \left(-(2x + 1)\right)^{3/2}. \tag{27}$$

Consequently there is a cusp at $x = -1/2$ which locally looks like a half plane extending to the left. This is an example of a vertex singularity so that the analysis of the previous
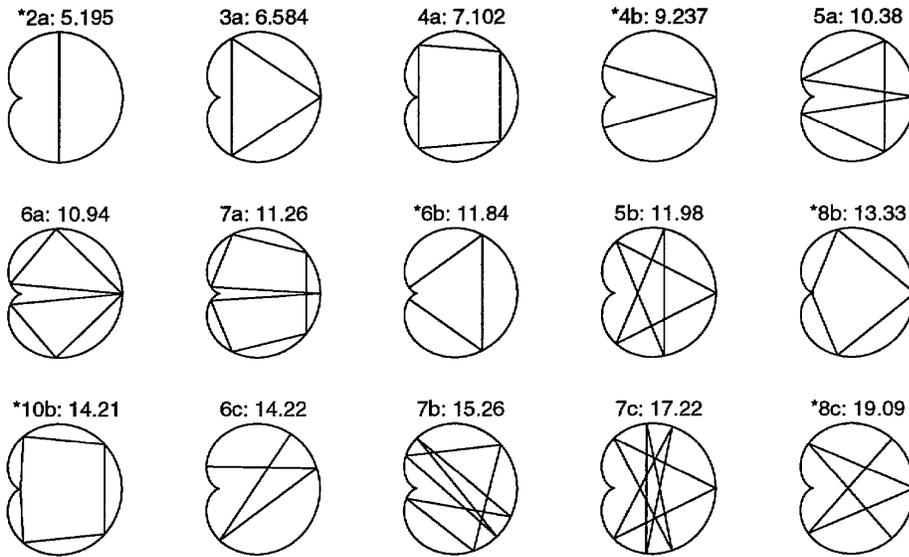
**Figure 3.** Various geometric orbits of the cardioid billiard labeled with their names and their lengths.
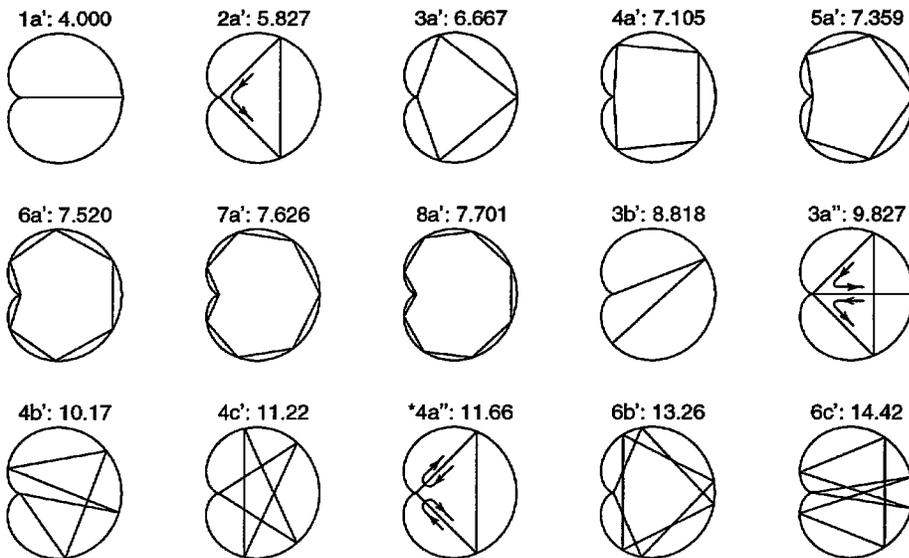
Figure 4. Various diffractive orbits of the cardioid billiard labeled with their names and their lengths. We indicate the incoming and outgoing directions where it is ambiguous.

section applies.

We found periodic orbits numerically by using the principle of least action. For an arbitrary periodic orbit the number of intersections with the boundary was specified and the intersection positions were varied until a local minima of the total orbit length was

found. Diffractive orbits were found the same way but with the constraint that one of the intersections was at the cusp. Various geometric orbits are shown in figure 3. The label of each orbit includes the number of intersections and also a letter index to further distinguish them. We describe a better naming system below. The asterix designates self-dual orbits as defined below. In figure 4 we show various diffractive orbits. The naming scheme is similar to before, the number gives the number of bounces—not counting the cusp. The primes indicate diffractions, ie. the number of encounters at the cusp. Orbits 2a', 3a'' and *4a'' have arrows drawn to indicate the scattering directions at the cusp. The last two have two diffractions and 3a'' is seen to be a composition of 1a' and 2a'
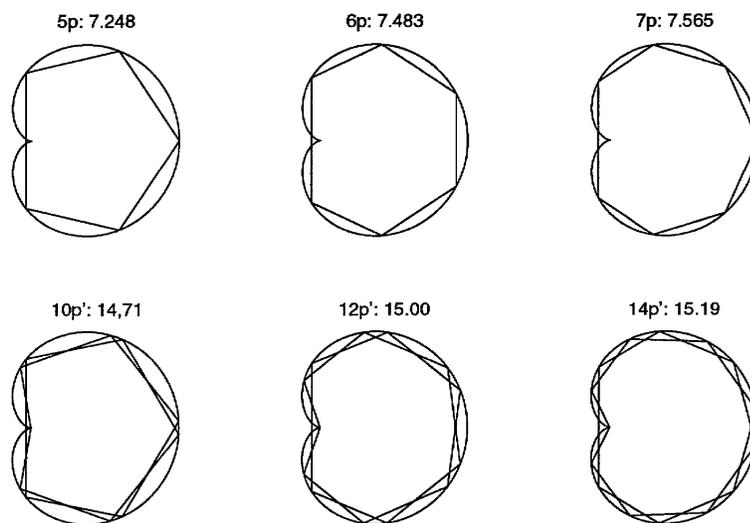
Figure 5. A family of related pruned geometric orbits and pruned diffractive orbits labeled with their names and their lengths.

The three orbits *6b, *8b, and *10b are geometric and reflect specularly near the cusp, contrary to appearances. Also, 4a misses the cusp and is geometric in contrast to 4a' which hits the cusp and is diffractive. In figure 5 we show examples of pruned orbits [40] of both the geometric and the diffractive kind. These have an index p in their label to indicate that they are pruned. It can be seen that the orbits are related pairwise; orbit 10p' appears to be composed from 5p and 5a' and similarly for 12p' and 14p'. This is a feature we discuss below.

3.2. Symbolic dynamics

Symbolic dynamics [28] is the partitioning and labeling of topologically distinct regions of phase space. Because of the reflection symmetry of the problem, we can discuss the dynamics either in the full domain or in just half of it. The half domain, also called the fundamental domain, has dynamics which are the same as in the full domain but with a reflection at the symmetry axis. We will show that the full and fundamental domains have distinct but closely related symbolic dynamics. We begin with a discussion of the symbolic dynamics of the geometric orbits.

For an arbitrary, time-reversal invariant system with a reflection symmetry, all orbits

belong to one of five classes. In principle there can be boundary orbits which lie directly on the symmetry axis; in this example there happen to be no such geometrical orbits. The other four possibilities are (i) symmetric and self retracing, (ii) symmetric but not self-retracing, (iii) self-retracing but not symmetric, and (iv) neither self-retracing nor symmetric. These occur with multiplicities 1, 2, 2 and 4 respectively and examples are *4b, 3a, 6c, and 7b. Although (iv) is the most generic possibility, we did not find many examples of it among the shortest orbits. It is typical that the shortest periodic orbits are special [41, 42] and that generic ones begin to appear only for longer lengths. Orbits of classes (ii)–(iv) behave identically in the half domain as in the full domain. Orbits of class (i), the so-called self-dual orbits, must be treated more carefully because in the fundamental domain they are periodic in $T_\gamma/2$ as well as in T_γ.

We start by discussing the symbolic dynamics of the full domain. Recalling that each point on the boundary of the billiard is labeled by an angle θ in (25), we assign a trajectory the symbol '+' every time it has a reflection which increases θ (counterclockwise) and the symbol '−' every time it has a reflection which decreases θ (clockwise). At the cusp, the angle θ changes discontinuously by 2π, so it defines what we mean by an increase or decrease of angle. Since we allow no geometric orbit to hit the cusp, it is not a problem that the sign of θ is not defined there. This is a general property of dynamical systems—the symbolic dynamics is often conveniently described with reference to a discontinuity [28].

As an example, consider orbit 3a. When going in the counterclockwise sense, it has the symbol sequence $+-+$. Its time reversed partner, which is distinct in the full domain, has the sequence $-+-$. We are free to start counting symbols anywhere on the orbit so that any cyclic permutation of a symbol sequence describes the same orbit and is not distinct. If W is the symbol sequence of an orbit which is symmetric under reflections (such as 3a) then $W = W^*$, where W^* is obtained by reversing the order of the symbols. For example, $+-+$ reads the same left to right as right to left. Self-retracing orbits of length $2n$ (they must be even) have symbol sequences with the structure $W = A\tilde{A}$ where A is some sequence of length n and $\tilde{A}$ is obtained from A by reversing the order and every sign. For example, the symbol sequence for the self-retracing orbit 6c is $--+-++$ for which $A = --+$ and $\tilde{A} = -++$. A self-dual orbit is both symmetric and self-retracing and therefore its symbol has both properties. An example is *4b whose symbol sequence is $++--$ (this satisfies the property of being symmetric if one makes use of the freedom to cyclically permute the symbols.)

The symbolic dynamics in the fundamental domain are defined by looking at the symbol sequence of an orbit in the full domain and assigning a 0 if two adjacent symbols are the same and a 1 if they are not. For example, orbit 3a, which is labeled $+-+$ in the full domain is 011 in the fundamental domain. The time reversed orbit in the full domain, $-+-$, is also 011 in the fundamental domain. This is consistent since in the full domain they are distinct and should have separate symbols while in the fundamental domain they are not distinct and should have the same symbol.

Note that a self-dual orbit in the full domain has a symbol sequence in the fundamental domain which repeats itself, for example *4b has the sequence $0101 = (01)^2$. Therefore a self-dual orbit, when mapped onto the fundamental domain, is the double repeat of a shorter orbit. Every odd multiple of this shorter orbit will be present in the fundamental domain but not in the full domain and this is apparent in the symbolic sequences. Any sequence in which 1 appears an odd number of times can not be periodic in the full domain and so corresponds to a self dual orbit. Any orbit which is symmetric in the full domain is self-retracing in the half domain.

We show in table 1, the symbols of all orbits up to length 4 as measured in the

Table 1. Some geometric orbits and their symbols.

Orbit	Full domain	Fundamental domain
2a	$+-$	1
4b	$+-+-$	$0101 = (01)^2$
3a	$+-+$	011
6b	$+++---$	$001001 = (001)^2$
4a	$+++-$	0011
8b	$++++----$	$00010001 = (0001)^2$
8c	$+--+-++-$	$10111011 = (1011)^2$

fundamental domain. There is no fundamental orbit 0, this is reminiscent of the co-linear helium problem [10], among others. The pruned family 5p, 6p, 7p... means that there are no orbits with the symbol sequence 0^n11 with $n > 2$. On the other hand, there is an accumulation of whispering-gallery-like orbits labeled 5a, 6a, 7a... whose symbol sequences have the form 0^n101 and whose lengths accumulate to $L = 12$ as $n \to \infty$. There are also orbits of the form 01^n; for n even they are 3a, 5b, 7c... while for n odd they are self-dual and are 4b, 8b,... We believe that both series exist for any n.

The symbolic dynamics of diffractive orbits is clearest if one think of the cusp as not being part of the boundary but rather being a means of getting from one point on the boundary to another. We introduce a symbol d which represents a path between two points on the boundary which goes via the cusp and keep $+$ and $-$ as defined above. Therefore, orbit 2a' has two boundary intersections and has a symbol sequence $d+$ or $d-$ depending on the sense of the rotation. Symmetric diffractive orbits labeled dW satisfy $W = W^*$ while self retracing orbits have the structure $W = A\tilde{A}$, as for geometric orbits.

The rule for the symbolic dynamics in the fundamental domain is again found by looking at the word in the full domain. A symbol $d \mapsto d$, while a $+$ or $- \mapsto 0$ or 1 depending on whether the next non-d symbol is the same or different. For example, in the half domain, 2a' has the symbol $d0$. In the fundamental domain, the two rotation senses of 2a' are not distinct and it is consistent that there is only one symbol sequence. The geometric orbits discussed above can be subsumed into a larger ternary alphabet in which they are the subclass with no d in their symbol sequence.

As before, any symbol sequence with an odd number of 1's must correspond to half of a self-dual orbit. However, self-dual orbits with one diffraction have the special property of being geometrically identical to a non-self-dual diffractive orbit and we refer to the pair as complements. An example of this is the self-dual orbit *4a" which is a perfect overlap of orbit 2a', the only difference being that the first backscatters at the cusp while the second forward scatters. Consequently, *4a" has twice the length of 2a' and suffers two diffractions rather than one. This is general, the self-dual orbit always leaves the cusp at an angle which is the negative of its complement and then follows a trajectory which is simply the reflection of its complement. If an orbit in the full domain has the symbol sequence dW then its self dual complement has the symbol sequence $dWdW'$ where W' is defined such that WW' satisfies the self-dual property. For example, *4a" has the symbol sequence $d+d-$ and $+-$ is clearly self-dual. In the fundamental domain the symbol sequence of a self-dual orbit is found from its complement by switching the symbol immediately before the d. For example, the symbol sequence of 3b' is $d11$ while that of its self dual complement (not shown) is $d10d10$ (recall that due to the cyclic symmetry, the last character in these

sequences is 'before' the d). In table 2 we show the labels of all singly diffractive orbits up to length 4. Note that the symbols $d101$ and $d011$ are simply time-reversed copies of each other and contribute equally to the trace.

Table 2. Some diffractive orbits and their symbols.

Orbit	Full domain	Fundamental domain
1a'	d	d
2a'	$d+$	$d0$
4a''	$d+d-$	$d1d1 = (d1)^2$
3a'	$d++$	$d00$
3b'	$d-+$	$d11$
4a'	$d+++$	$d000$
4c'	$d+-+$	$d110$
4b'	$d+--$	$d101$

   To find the symbol sequence of any multiply diffractive orbit, we use the same rule. For example, the doubly diffractive orbit 3a'' starts at the cusp, travels along 1a' back to the cusp, diffracts onto the 2a' orbit, travels along 2a' back to the cusp and finally diffracts onto the 1a' orbit in the original direction. Its symbol sequence is $d0d$. Because there is only one vertex, the only multiply diffractive orbits are compositions of singly diffractive ones. More possibilities would exist if there were more than one vertex.

   If all possible symbol sequences were realized as orbits, the number of singly diffractive orbits in the fundamental domain up to length n would grow as 2^n. For geometric orbits with a complete binary alphabet, the number grows as $2^n/n$. The factor of n in the denominator is because cyclically permuted symbols correspond to the same orbit and should be counted only once. It appears that there are more singly diffractive orbits of long length and it is not clear if they ultimately dominate the spectrum. A related issue is whether the pruning of geometric and diffractive orbits is such that the exponential proliferation of the two classes of orbits is given by the same exponent. This is quite likely since very long orbits cover the phase space uniformly and are therefore susceptible to the same pruning mechanisms as shown in figure 5. These questions will be studied in greater detail in a later publication [43] and here we have just a brief discussion.

   The pruning of geometric and diffractive orbits appear to be strongly correlated. For example, the pruned diffractive orbit 10p' looks as if it is composed of the pruned orbit 5p and the diffractive orbit 5a'. This is confirmed by looking at the symbol sequences of these three orbits. Orbit 10p' has the word $d++++-++++$ which is equal to the composition of those for 5a' and 5p which are $d++++$ and $-++++$, respectively. A similar result holds for orbits 12p' and 14p'. Usually, the existence of pruning implies problems in the cycle expansion of the zeta function due to the breakdown of shadowing [28] so the fact that orbits and their shadows have disappeared together might prove very useful. An example of non pruned shadowing are $5b \Leftrightarrow 2a + 3a$ (since $+-++- = +-||++-$) and $4c' \Leftrightarrow 2a' + 2a$ (since $d+-+ = d+||-+$).

   The symbolic dynamics was useful to us in guessing the topology of a few missing orbits. However, we did not make extensive use of it as we were content to know the shortest orbits and these can be found by trial and error. It is useful, however, in the following discussion of Maslov indices and symmetry reduction. In addition, a project which required knowing many orbits, such as attempting to find semiclassical approximations to many quantum eigenvalues, would need to make extensive use of the symbolic dynamics.

3.3. Maslov indices

In this subsection we discuss the Maslov indices which appear in the trace formulae (1) and (17), beginning with the geometric indices. Starting at an arbitrary point, x, on the orbit, the index σ_γ equals the number of caustics μ plus an index ν which arises on doing the stationary phase integral in the determination of the trace. Although μ and ν depend separately on the point x along the orbit, their sum does not. In fact, σ_γ is a canonical invariant [20] which equals twice the number of times that the stable and unstable manifolds wind in completing one circuit of the periodic orbit. It follows that we can use any point x on the orbit to calculate σ_γ.

We numerically propagated the 2×2 monodromy matrix, M, for each geometric orbit and counted the number of caustics μ by the number of times that one of the off diagonal elements M_{12} changed sign. At the end, we also found the value of $(\mathrm{Tr}M - 2)/M_{12}$; if it is positive $\nu = 0$ and if it is negative $\nu = 1$. Doing so, we found the following simple topological rule; σ_γ equals the number of reflections or, equivalently, the length of the symbol sequence of that orbit. This rule probably arises from the fact that the cardioid is a purely defocusing billiard so there is, on average, one focus per reflection. In the Bunimovich stadium, one finds a similar rule that σ_γ is incremented by one for each reflection off the defocusing end caps [44]. It is common that such a simple rule exists and it is usually related in some simple way to the symbolic dynamics.

For the diffractive orbits, σ_γ is the number of caustics between successive diffractions. We found that σ_γ always equals the number of geometric reflections and hence the length of the symbol sequence, as before. This appealing result implies a unity between the two classes of orbits.

Every geometric reflection also induces a sign change due to Dirichlet boundary conditions. We account for this by incrementing σ_γ by 2 at every reflection, so that in total $\sigma_\gamma = 3m_\gamma$ where m_γ is the number of reflections experienced by orbit γ. For Neumann boundary conditions this is not necessary, and $\sigma_\gamma = m_\gamma$. Consistent results, specialized to the half cardioid, were obtained in [36].

3.4. Symmetry decomposition

The billiard has a reflection symmetry C_2 and consequently all quantum states can be classified as even or odd. The trace decomposes as

$$g(E) = g_+(E) + g_-(E). \tag{28}$$

We can separately find $g_\pm(E)$ by studying the dynamics in the fundamental domain and from them the densities $\rho_\pm(E)$. The behaviour of the geometric trace formula (1) under symmetry decomposition is a well studied problem [41, 42, 45, 46] and here we review the results which are relevant to us. Thereafter, we discuss the decomposition of the diffractive trace formula, which is slightly different.

The non-self-dual orbits have multiplicities of either 2 or 4 in the full domain and their amplitudes are divided equally between the two parity classes. Self-dual orbits require more care. Half of such an orbit, being periodic in the fundamental domain, contributes to the the separate traces as follows. Its period, stability and Maslov index are all half of the full orbit and its stability is the square root. In addition the $\mp$ factor in the denominator of (1) is replaced by $\pm$. Finally, there is a group theoretical weight of $\pm$ corresponding to the even/odd parity. This last factor ensures that the contribution of this half orbit identically cancels when we evaluate the sum $g(E) = g_+(E) + g_-(E)$. This is consistent since the half orbit is not a periodic orbit of the full domain and should not affect the total density of

states. The double repeat of a half orbit is the full orbit and its amplitude is divided equally between the two parities.

   We next discuss what happens to the diffractive orbits in the presence of the symmetry. There is a diffractive boundary orbit; it contributes only to the even spectrum [7, 9, 41], unlike a geometrical boundary orbit which contributes to both. The distinction can be traced to the fact that the diffractive Green function (2) is multiplicative in the direct Green functions. For the other diffractive orbits, we recall the previous discussion that each of them has a self dual complement of twice the length. The only difference between the orbits in the fundamental domain is that they have different diffraction constants. If one has the diffraction constant $d(\theta, \theta')$ the other has the diffraction constant $d(-\theta, \theta')$. Since they are in all other respects identical, we can include both of them by defining separate diffraction constants for the even and odd parities, namely

$$d_{\pm}(\theta, \theta') = d(\theta, \theta') \pm d(-\theta, \theta'). \tag{29}$$

The different sign for the two cases is the same group theoretical weight mentioned for self-dual geometric orbits.

   As mentioned above, for the half plane and for Dirichlet boundary conditions, $d(-\theta, \theta') = d(\theta, \theta')$ so we have

$$d_{+}(\theta, \theta') = 2d(\theta, \theta') \qquad d_{-}(\theta, \theta') = 0. \tag{30}$$

This implies that the odd spectrum is completely insensitive to the existence of diffraction. For wedges which are not half-planes, (30) is not true but it will still be true that (29) will cause the two parities to be affected differently. If we study the billiard with Neumann boundary conditions we reach the opposite conclusion. First, the boundary orbit has zero amplitude since (4) implies that $d(0, 0) = 0$ in that case. Also, $d(-\theta, \theta') = -d(\theta, \theta')$ for Neumann boundary conditions so that

$$d_{+}(\theta, \theta') = 0 \qquad d_{-}(\theta, \theta') = 2d(\theta, \theta'). \tag{31}$$

Therefore, the odd spectrum would have diffractive peaks and the even spectrum would not.

3.5. Weyl formula

The Schrödinger equation for a billiard reduces to the Helmholtz equation

$$\left(\nabla^2 + k^2\right) \psi(r) = 0 \tag{32}$$

with Dirichlet, Neumann or mixed boundary conditions on the boundary of the domain. Finding the eigenvalues k_n^2 leads to the density of states $\rho(k) = \sum_n \delta(k - k_n)$. One commonly decomposes this into a smooth part and a fluctuating part

$$\rho(k) = \bar{\rho}(k) + \rho_{\text{fl}}(k). \tag{33}$$

These terms have distinct classical interpretations. The first term, commonly called the Weyl term, is related to the geometry of phase space, such as the area, perimeter, curvature and other properties of the billiard boundary. The second term is given by the dynamics as encoded in the trace formulae (1) and (17). Actually, each term of (33) is an asymptotic expansion in powers of $1/k$ [47]. To date, the first 16 terms of the expansion of $\bar{\rho}(k)$ have been calculated but here we make ourselves content with the first three. Additionally, the first corrections to $\rho_{\text{fl}}(k)$ have also been determined [48, 49] but we do not consider them here.

Instead of $\bar{\rho}(k)$, one often refers to the spectral staircase function $\bar{N}(k)$ of which $\bar{\rho}(k)$ is the derivative. Its expansion for Dirichlet boundary conditions is (see for example [47])

$$\bar{N}(k) \approx \frac{A}{4\pi} k^2 - \frac{L}{4\pi} k + C - \cdots \qquad (34)$$

where A is the area of the billiard, L is the length of the perimeter, and C is related to the curvature and to corners by

$$C = \frac{1}{24\pi} \sum_i \frac{\pi^2 - \theta_i^2}{\theta_i} + \frac{1}{12\pi} \int \kappa(s) \, ds. \qquad (35)$$

The sum is over angles in the billiard boundary; we have one angle of 2π. The integral gives the total curvature over the boundary of the billiard. Note that (34) also applies to billiards with Neumann boundary conditions if we multiply every other term by -1. For the full spectrum, we find $A = 3\pi/2$, $L = 8$ and $C = 3/16$. We can also use (34) for the odd spectrum by taking the billiard domain to be the fundamental domain. We then have $A = 3\pi/4$, $L = 6$ and $C = 3/16$. The difference between the total spectrum and the odd spectrum must correspond to the even spectrum, so for it we have $A = 3\pi/4$, $L = 2$ and $C = 0$. The symmetry decomposition of the Weyl formula for billiards was discussed in much greater generality in [50]. These results for the cardioid billiard were also obtained in [36].

Comparing the exact staircase functions with the approximation (34) is a useful check that there are no missing levels. In addition, the point where there the curves start to deviate is a useful criterion for establishing when the numerical eigenvalues are no longer reliable. The Weyl formula is also needed to compare the Fourier transforms of the data and the trace formulae in section 4 and also to renormalize the spectrum for the statistical analysis of section 5.

4. Numerical results

In this section we present comparison between the exact spectra and the results of periodic orbit theory. We first do this by directly comparing the Fourier transforms of the exact spectra and the trace formulae in the reciprocal space of orbit lengths, L. Overall, there is good agreement and we successfully reproduce geometric, diffractive and doubly diffractive peaks as well as the interferences among them. However, there is a region of L which is not well reproduced for reasons we explain. We also find that for other regions of L, the exact diffractive peaks have magnitudes larger by a few percent than what we expect. We explain this by recalling that the cusp is not a perfect vertex. Finally, we use the sum over periodic orbits to find the first few quantum eigenvalues and find the odd result that including diffractive orbits seems to shift them only slightly.
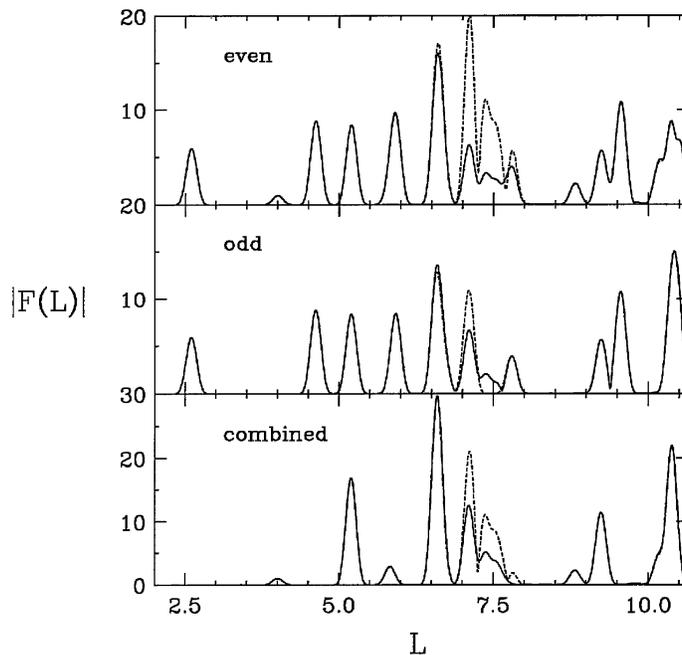
4.1. Fourier transforms

Using the algorithm of [33] we truncate the Hilbert space to contain only the lowest 6600 states and calculate the lowest 1000 eigenstates of each parity with an accuracy better than 0.001 times the average level spacing. It is these 2000 states we use in the analysis. For a precise comparison, it is best to work with $\rho_{\text{fl}}(k)$ which is obtained from subtracting the Weyl term $\bar{N}(k)$ of (34) from the exact density of states. We obtain its Fourier transform as

$$F(L) = \int_{-\infty}^{\infty} dk \, w(k) [\rho(k) - \bar{\rho}(k)] e^{ikL} \qquad (36)$$

where $w(k)$ is a window function. We chose to use the 3-term Blackman–Harris window [51] which gives a good compromise between narrowness of peaks and smallness of side lobes. This is defined as

$$w(k) = \sum_{j=0}^{2} a_j \cos\left(2\pi j \frac{k - k_0}{k_1 - k_0}\right). \tag{37}$$

where $(a_0, a_1, a_2) = (0.42323, -0.49755, 0.07922)$. This function goes smoothly to zero at k_0 and k_1 which we choose as the of the first and last eigenvalues in our spectrum.

Figure 6. The solid curves are the Fourier transforms of the exact spectra and the dashed curves are the approximations from the trace formulas (19) and (20).

We apply the same Fourier transform to the trace formulae (19) and (20) to obtain the semiclassical approximation $F_{\text{SC}}(L)$. We included all relevant period orbits with $L < 11$; the most was for the even spectrum which had 38 orbits, including halves of self-dual orbits and multiple repeats of 2a. The results up to $L = 10.7$ are shown in figure 6 for the even, odd and combined spectra. Other than the region around $L = 7.5$ which we discuss later, the agreement is very good. This was also observed in [8] but here we are also verifying the geometrical factors F in (19). Note that there are no diffractive peaks in the odd spectrum as we argued above. The geometric peaks in the even and odd spectra near $L = 2.5$, $L = 4.7$, $\cdots$ are halves of self-dual orbits and are absent in the full spectrum.

We stress that the relative heights of the diffractive peaks are artifacts of the range of the quantum spectrum we choose to consider and should not be used to estimate the relative weight of these orbits in determining quantum eigenvalues. The reason is that they are suppressed as $1/\sqrt{k}$ and contribute more and more weakly to the energetic states. However, their effect in the ground state region can be quite large – a possibility we explore later.

We now turn our attention to the large discrepancy near $L = 7.5$. There are two distinct reasons why the trace formulas fail there. The first is that orbits 4a, 4a' and *10b are close in configuration space and interfere differently than we have assumed up to now. The second reason is that the cusp is only approximately a half-plane vertex. To understand the first point, we appeal to the calculation which gives the diffraction constant. Sommerfeld [15] showed that an incoming plane wave is broken up by a half plane vertex into three components; a plane wave which continues in the original direction, another plane wave coming from reflection off one face, and a third component which he identified as the diffracted field. The diffracted field is asymptotically an outgoing circular wave of the form $f(\theta) \exp(ikr)/\sqrt{kr}$ and the diffraction constant d is proportional to $f(\theta)$. However, in the directions close to the two out going plane waves, the diffracted wave takes longer and longer to obtain its asymptotic form and exactly in the plane wave directions it never does. It is this attempt to connect to the incorrect asymptotic form in these two directions which leads to the divergence of (3) when $\theta \pm \theta' = \pi$. Ideally, one would like to have a uniform approximation to cover all ranges of θ and θ'. In the case discussed here, we will find that the approximation improves as k increases.

The second reason for the failure of the trace formula near $L = 7.5$ is that the billiard domain departs relatively rapidly from its local half plane geometry at the cusp so that the diffraction constants derived assuming a half plane may not be appropriate. In fact, this approximation is fine for orbits which come in from the right, such as 1a', since they are never close to the faces of the cusp. However, orbits entering the cusp from the left, such as 5a', are very sensitive to this approximation. The curvature of the boundary means that such orbits are not as far from the boundary as is assumed in the calculation of the diffraction constant so that the Dirichlet boundary conditions cause more suppression than is accounted for.

To understand this another way, note that for any finite wavenumber, k there is not infinite spatial resolution so the cusp appears as a finite angled wedge. However, a finite angled wedge has different diffraction constants. Therefore, it is reasonable to suppose that at small wavenumbers the lack of resolution, inherent in the finiteness of k, manifests itself as inaccuracies of peak amplitudes in the Fourier spectra. We explored this effect for orbit 1a' by looking at two windows of k. For this study, it is best to use the combined spectrum because then there is no interference from the self-dual orbits 2b and 4b. We are extremely sensitive to errors because we are interested in the difference between two small peaks. Accordingly, we use just the lowest 285 states which are extremely accurate (approximately 140 of each parity) which we divided into two windows of approximately equal extent in k (2.01–26.32 and 13.09–39.39 respectively with means $\langle k \rangle = 14.17$ and 26.24.) The comparison between the numerics and the trace formula (19) is shown in figure 7. In both cases, we find that the exact spectrum has a peak which is slightly larger than predicted but that the discrepancy is larger by about 50% for the first window.

This strengthens our argument that the large discrepancies around $L = 7.5$ in figure 6 arise because the orbits responsible for those peaks are sensitive to the fact that the cusp is not a true half plane. We argue that because they approach the cusp from the left they are far more sensitive to this than orbits approaching from the right. Furthermore, such orbits are probably sensitive to the entire curved geometry in the neighbourhood of the cusp.

The fact that there is structure in the odd spectrum with lengths the same as for diffractive orbits (particularly visible near $L \approx 7.5$, an effect also observed in [36]) is not unexpected. In one of their seminal papers, Balian and Bloch [21] argued that for a billiard domain, with a discontinuity in the nth derivative of the boundary, there exists contributions to the density of states of order $\hbar^{n/2}$. For sharp corners, we have $n = 1$ and this conforms to
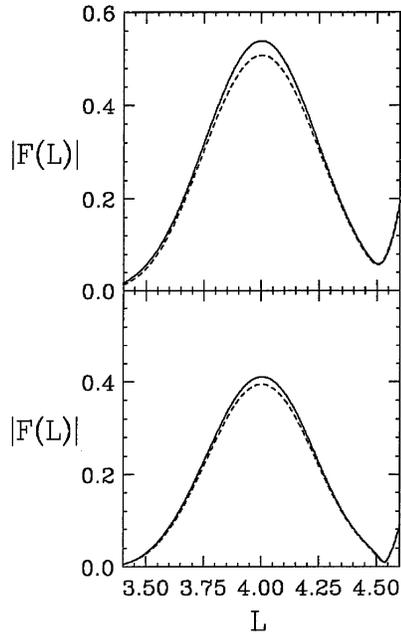
Figure 7. Comparison between the exact result (solid curve) and the diffractive trace formula (dashed curve) for orbit 1a'. The top box is the window $2.01 \leqslant k \leqslant 26.32$ and the bottom box is the window $13.09 \leqslant k \leqslant 39.39$.
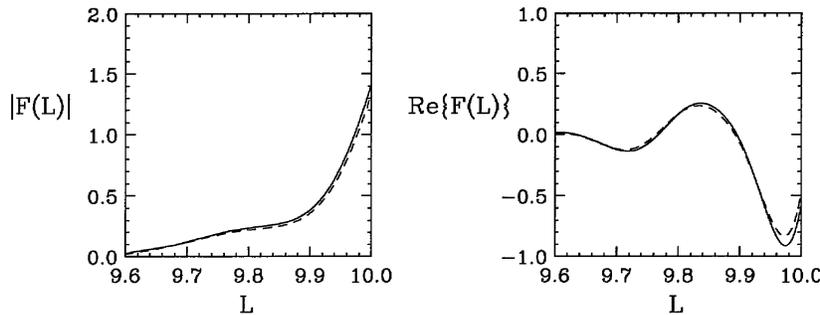

Figure 8. As in figure 6 but for a range corresponding to the double diffractive orbit 3a''.

the previous discussion. For discontinuous changes in the curvature we have $n = 2$. The second case applies here for the odd spectrum since the half cardioid has continuous slope but its curvature changes discontinuously from zero to infinity at the vertex. Normally, this structure is too small to be visible but we suppose that the geometrical considerations which amplify the diffractive peaks in the even spectrum have a similar effect on the higher order peaks in the odd spectrum.

Another possibility for contributions due to a change in curvature is discussed in [4, 5] in the context of the Bunimovich stadium [37]. It was found that although one can unambiguously continue a classical trajectory which encounters the discontinuity, the stationary phase integral to evaluate its contribution to $\rho(E)$ requires more care. This is

because the character of the motion is different on each side of the orbit. This applies to orbits which reflect specularly at the vertex and so are geometrical, not diffractive.

Finally, we discuss the small peak near $L = 9.8$ corresponding to orbit 3a". We use (19) with the appropriate diffraction constants. To eliminate interference from the nearby self-dual peak 8c we analyse the combined spectrum. Because this is such a small peak, it is particularly sensitive to small backgrounds. One source of background is slight errors in the determination of the exact quantum energy levels; such errors manifest themselves as weak oscillations in the Fourier transforms. For this reason, we used only the lowest 1000 levels. In figure 8, we show both the absolute value of the Fourier transform and its real part. The discrepancy, which grows towards the right of the figure, comes from a slight error in the peak amplitude of 4b'.
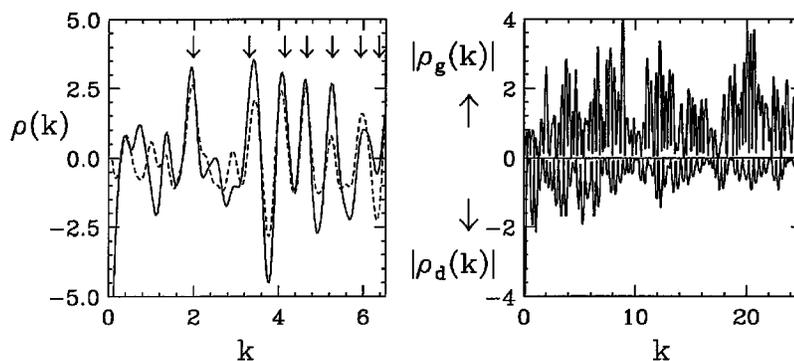
Figure 9. Left: The solid curve is the result of using both geometric and diffractive orbits in the trace formula for the even spectrum while the dashed curve is from using just the geometric orbits. The arrows denote the exact positions of the even states. Right: A comparison of the magnitudes of the geometric (top) and diffractive (bottom) contributions to the density of states.

4.2. Recovering quantum eigenvalues

The trace formulae (19) and (20) can be used to find quantum eigenvalues. Here we do this with and without the diffractive orbits to see what effect they have on the determination of the eigenvalues. We simply summed over the orbits used to obtain figure 6. Because of the problems with the diffractive orbits 5a', 6a' ... we ignored that series of orbits. Additionally, we made an approximate fix for small k of the orbits 4a, 4a' and *10b by ignoring 4a' and *10b and halving the amplitude of 4a. This simulates the effect of the cusp which has the approximate effect of halving the domain of the stationary phase transverse integral used to derive the geometrical trace formula. The result for the even spectrum is shown in figure 4.1 with and without diffractive orbits. The peaks are identified as corresponding to quantum eigenvalues. We observe that including diffraction helps to resolve the peaks but barely changes their positions. The positions are compared in table 3. The discrepancy is typically 0.06 compared to a spacing of about 0.80. Including the diffractive orbits changes the peak positions only by about 0.02 and not necessarily by the correct sign.

This is a strange result because the amplitude of the geometric and diffractive contributions to the density of states are comparable, as shown in the right half of figure 9. We saw in the previous section that the eigenvalues do contain information about diffraction since there were diffractive peaks in the Fourier transform so it must be true that the

Table 3. Top: even states calculated with and without diffractive orbits. Bottom: odd states.

State number	Exact eigenstate	Geometric orbits	Geometric and diffractive orbits
1	2.010	1.956	1.943
2	3.331	3.434	3.406
3	4.169	4.053	4.070
4	4.686	4.629	4.618
5	5.292	5.238	5.248
1	3.020	2.979	—
2	4.160	4.134	—
3	5.162	4.999	—
4	5.558	5.356	—
5	6.174	6.133	—

diffractive orbits have some effect on the eigenvalues. To unravel this paradox it is probably best to calculate with zeta functions rather than traces, which we will do in a later publication [43]. For now we note that the wedge billiard was also successfully quantized using only geometric orbits although it too has a diffractive vertex [23].
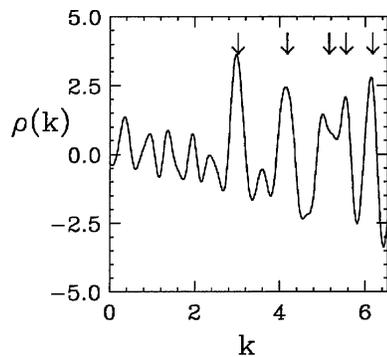

Figure 10. The odd density of states as constructed from just the geometric orbits and the arrows denote the exact positions of the odd states.

For completeness, we show in figure 10 the results for the odd spectrum and the results are also enumerated in table 3. Now only geometric orbits contribute. The agreement is somewhat better; with the exception of the third state, which is not well resolved in any case, the differences between the peak positions and the quantum eigenvalues are typically about 0.04. The only qualitative difference between the two parities is the diffraction so the difference in accuracy is presumably diffraction related.

5. Spectral statistics

It is by now well known, if not well understood, that the statistics of eigenvalues of chaotic systems [52] follow closely the predictions of random matrix theory (RMT) (for a review see [53]). This has been confirmed in many examples including the conformal mapping

of the circle [33] of which the cardioid is a limiting case. Nevertheless, we repeat this here to see if the diffraction has any effect on the statistics. The fact that the diffraction is almost completely limited to the even spectrum means that we can study its relative effect by comparing the results for the even and odd spectra. A similar study was already reported in [36] for the half cardioid but without an explicit comparison of the odd and even spectra to explore possible diffraction effects.
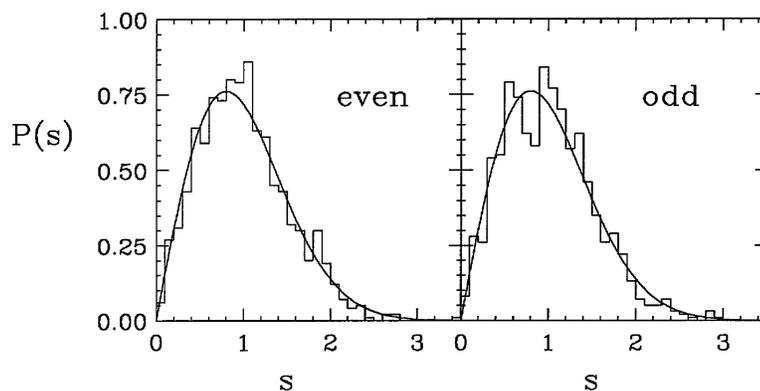
Figure 11. Histograms showing the spacing distributions of the even and odd spectra. The solid curve is the GOE result.

We first display the spacing distributions in figure 11. This is the distribution of the spacings s between adjacent energy levels measured in units of the local mean level density as found from the Weyl formula (34). The Gaussian orthogonal ensemble (GOE) is a random matrix ensemble which predicts a spacing distribution very close to

$$P(s) = \frac{\pi}{2} s \exp(-\pi s^2 / 4). \tag{38}$$

Both spectra are observed to be consistent with that limit and with each other so diffraction appears to have no significant effect on the spacing distribution.

The spacing distribution is a measure of short range correlations. A statistic commonly used to probe the long range correlations is the spectral rigidity $\Delta_3(l)$. Here l refers to distances in the spectrum measured in units of the mean level spacing. (We use a small letter l to avoid confusion with the periodic orbit lengths which we referred to with a large L.) This statistic measures the average χ^2 deviation of the staircase function from a local straight line fit over a window of length l; the average being taken as the window is moved through the spectrum. The GOE formula is given as a complicated integral representation but for large l is nearly $(\log l)/\pi^2$. Chaotic systems follow the GOE result [54] but at some point begin to deviate from it and finally saturate for arguments larger than about $l_{\max} = 2\pi \langle \rho(k) \rangle / L_{\min}$ where $\langle \rho(k) \rangle$ is the average level density and $L_{\min}$ is the length of the shortest periodic orbit. The shortest periodic orbit in the cardioid is 2a which has length 2.60 in the fundamental domain. The average density of states in the range considered is 20.0 so that $l_{\max} = 48.3$.

In figure 12, we show the $\Delta_3(l)$ results for the even and odd spectra. We also show the saturation value of 0.265 which we found numerically. As can be seen, $l_{\max}$ is a good approximation to where the saturation begins. The results are significantly different from the GOE prediction for values of l larger than about 7. In comparing the two data sets, we observe that the odd spectrum has values which are consistently larger than the even
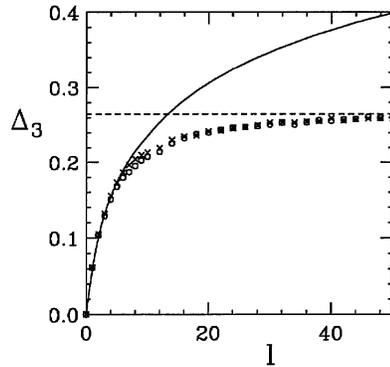
Figure 12. The $\Delta_3(l)$ functions for the even ($\circ$) and the odd ($\times$) spectra. The solid curve is the GOE result and the dashed line denotes the saturation value.

spectrum for $0 < l < 17$. The difference is typically about 0.01. To determine if this is significant we need to compare the difference to the typical variance in $\Delta_3(l)$. If we assume that each range of length l used in determine $\Delta_3(l)$ is statistically independent, we find that the typical variance is 0.006. This assumption is problematic since we know that there are strong correlations in the spectra. If instead we determine the variance by finding the effect of removing selected levels, then the typical variance is 0.02 [55]. In either case, we conclude that if there are significant deviations between the two spectra, we are not sufficiently sensitive to resolve them with confidence. This conclusion is in agreement with the results of the wedge billiard [23] and of pseudo-integrable billiards [56]. We can increase the statistical significance of this statement by finding more eigenvalues. It would also be interesting to study this question analytically by extending the Berry's original semiclassical calculation of spectral rigidity [54] to include the effect of diffractive orbits.

6. Conclusion

In this paper, we have derived a trace formula for periodic orbits diffracted by vertices. The presence of the diffractive orbits causes additional structure in the quantum spectra of Hamiltonian systems. This structure is suppressed relative to the contributions from geometric orbits. The diffractive trace formula has a very similar structure to the trace formula for geometric orbits and from it we can find a zeta function in close analogy to the zeta function for geometric orbits. An important difference in the structure of these functions is that the diffractive zeta function involves only one product. Multiplying these zeta functions gives the total zeta function which will probably provide the cleanest method of finding the semiclassical eigenvalues.

We specialized the discussion to the example of the cardioid billiard possessing a cusp at the boundary which is locally a half-plane vertex. There is overall good agreement between the Fourier transform of the exact spectrum and that of the trace formulae and we successfully reproduced geometric, diffractive and doubly diffractive peaks as well as the interferences among them. However, there is a region of L which is not well reproduced. Two reasons for this disagreement are that for certain choices of angles the diffraction picture breaks down and because the cusp is not a perfect half-plane vertex.

There exists a symbolic dynamics which includes the periodic diffractive orbits in a

natural way by inclusion of one more symbol in the alphabet. This leads to a simple result when discussing the symmetry reduction. For every non self-dual diffractive orbit, there exists a complementary self-dual one. These interfere so that the diffraction affects only the even spectrum and leaves the odd spectrum alone. We used the sum over periodic orbits to find the first few quantum eigenvalues with an accuracy of a few percent. We found the puzzling result that including diffractive orbits seems to have very little effect. This issue will be addressed in a later publication.

In the last section we studied the level statistics of the even and odd spectra separately. Comparing the results from the two spectra is a probe of the effect of the diffractive orbits. This is because the odd spectrum has essentially no contribution from diffraction. We found no significant differences in either the spacing distributions or $\Delta_3(l)$ although we can not rule out the possibility that such differences might become apparent if we included more states.

Acknowledgements

Note added in proof. After submission of this paper, a preprint appeared [57] in which the symbolic dynamics of the cardioid are extensively explored. The results of that paper are consistent with those discussed here.

References

[1] Gutzwiller M C 1990 *Chaos in Classical and Quantum Mechanics* (New York: Springer)
[2] Wirzba A 1992 CHAOS **2** 77; Vattay G, Wirzba A and Rosenqvist P E 1994 *Phys. Rev. Lett.* **73** 2304
[3] Primack H, Schanz H, Smilansky U and Ussishkin I 1996 The role of diffraction in the quantization of dispersing billiards *Phys. Rev. Lett.* **76** 15
[4] Sieber M, Smilansky U, Creagh S C and Littlejohn R G 1993 *J. Phys. A: Math. Gen.* **26** 6217
[5] Alonso D and Gaspard P 1994 *J. Phys. A.: Math. Gen.* **27** 1599
[6] Vattay G, Wirzba A and Rosenqvist P E 1994 *Proc. Int. Conf. on Dynamical Systems and Chaos: Vol 2* ed Y Aizawa, S Saito and K Shiraiwa (Singapore: World Scientific)
[7] Whelan N D 1995 *Phys. Rev.* E **51** 3778
[8] Pavloff N and Schmit C 1995 *Phys. Rev. Lett.* **75** 61
[9] Whelan N D 1996 *Phys. Rev. Lett.* **76** 2605
[10] Richter K, Tanner G and Wintgen D 1993 *Phys. Rev.* A **48** 4182
[11] Seba P 1990 *Phys. Rev. Lett.* **64** 1855
[12] Date G, Jain S R and Murthy M V N 1995 *Phys. Rev.* E **51** 198
[13] Reimann S M *et al* 1996 *Phys. Rev. A: Math. Gen.* **53** 39
[14] Rosenqvist P E Whelan N D and Wirzba A 1996 *J. Phys. A: Math. Gen* at press
[15] Sommerfeld A 1896 *Mathem. Ann.* **47** 317; 1954 *Optics* (New York: Academic)
[16] Keller J B 1957 *Appl. J. Phys.* **28** 426
[17] Pauli W 1938 *Phys. Rev.* **54** 924
[18] Robnik M 1983 *J. Phys. A.: Math. Gen.* **16** 3971
[19] Markarian R 1993 *Nonlinearity* **6** 819
[20] Creagh S C, Robbins J M and Littlejohn R G 1990 *Phys. Rev.* A **42** 1907
[21] Balian R and Bloch C 1972 *Ann. Phys.* **69** 76
[22] Feynman R P and Hibbs A R 1965 *Quantum Mechanics and Path Integrals* (New York: McGraw-Hill)
[23] Szeredi T and Goodings D A 1990 *Phys. Rev. Lett.* **69** 1640 Szeredi T and Goodings D A 1993 *Phys. Rev.* E **48** 3529 Szeredi T, Lefebvre J H and Goodings D A 1994 *Nonlinearity* **7** 1463
[24] Creagh S C and Littlejohn R G 1991 *Phys. Rev.* A **44** 836

[25] Creagh S C and Dimon P 1996 *Geometrical orbits in the power spectra of waves* preprint
[26] Ruelle D 1978 *Statistical Mechanics, Thermodynamic Formalism* (Reading, MA: Addison-Wesley)
[27] Voros A 1988 *J. Phys. A.: Math. Gen.* **21** 685
[28] see for example, Cvitanović P 1988 *Phys. Rev. Lett.* **61** 2729; Artuso R, E Aurell and Cvitanović P 1990 *Nonlinearity* **3** 325; Artuso R, E Aurell and Cvitanović P 1990 *Nonlinearity* **3** 361
[29] Berry M V and Keating J P 1990 *J. Phys. A: Math. Gen.* **23** 4389
[30] see for example, Babi V Mć and Buldyrev V S 1990 *Short Wavelength Diffraction Theory* (Berlin: Springer)
[31] Berry M V and Robnik M 1986 *J. Phys. A.: Math. Gen.* **19** 649
[32] Hayli A, Dumont T, Moulin-Ollagnier J and Strelcyn J-M 1987 *J. Phys. A.: Math. Gen.* **20** 3237
[33] Prosen T and Robnik M 1993 *J. Phys. A.: Math. Gen.* **26** 2371
[34] Bruus H and Stone A D 1994 *Phys. Rev.* B **50** 18275
[35] Li B and Robnik M 1994 *J. Phys. A.: Math. Gen.* **27** 5509
[36] Bäcker A, Steiner F and Stifter P 1995 *Phys. Rev.* E **52** 2463
[37] Bunimovich L A 1979 *Commun. Math. Phys.* **65** 295
[38] Sinai Y G 1968 *Funct. Anal. Appl.* **2** 61, 245
[39] Bunimovich L A 1995 *Chaos* **5** 349
[40] Cvitanović P, Gunaratne G H and Procaccia I 1988 *Phys. Rev.* A **38** 1503
[41] Lauritzen B 1991 *Phys. Rev.* A **43** 603
[42] Cvitanović P and Eckhardt B 1993 *Nonlinearity* **6** 277
[43] Bruus H and Whelan N D to be published
[44] Creagh S C 1996 private communication
[45] Robbins J M 1989 *Phys. Rev.* A **40** 2128
[46] Creagh S C 1993 *J. Phys. A.: Math. Gen.* **26** 95
[47] Berry M V and Howls C J 1994 *Proc. R. Soc.* A **447** 527
[48] Gaspard P and Alonso D 1993 *Phys. Rev.* A **47** R3468
[49] Vattay G and Rosenqvist P 1996 *Phys. Rev. Lett.* **76** 335
[50] Pavloff N 1994 *J. Phys. A.: Math. Gen.* **27** 4317
[51] Harris F J 1978 *Proc. IEEE* **66** 51
[52] Bohigas O, Giannoni M-J and Schmit C 1984 *Phys. Rev. Lett.* **52** 1
[53] Mehta M L 1985 *Random Matrices and the Statistical Theory of Energy Levels* 2nd edn (New York: Academic)
[54] Berry M V 1991 *Proc. R. Soc.* **400** 229
[55] Lindemann K 1995 private communication
[56] Biswas D 1995 *Pseudo-integrable billiards - periodic orbits and spectral statistics* preprint
[57] Bäcker A and Dullin H R 1995 *The symbolic dynamics and periodic orbits for the cardioid billiard* preprint chao-dyn/9511004